

IMPROVING TISSUE ELASTICITY IMAGING USING A KALMAN
FILTER-BASED NON-RIGID MOTION TRACKING ALGORITHM

By

Susheel Reddy Vadde

Submitted in Partial Fulfillment of the Requirements for

The Degree of

Master of

Computing and Information Systems

YOUNGSTOWN STATE UNIVERSITY

May, 2011

IMPROVING TISSUE ELASTICITY IMAGING USING A KALMAN
FILTER-BASED NON-RIGID MOTION TRACKING ALGORITHM

Susheel Vadde

I hereby release this thesis to the public. I understand that this thesis will be made available from the OhioLINK ETD Center and the Maag Library Circulation Desk for public access. I also authorize the University or other individuals to make copies of this thesis as needed for scholarly research.

Signature:

Susheel Reddy Vadde, Student

Date

Approvals:

Dr. Yong Zhang, Thesis Advisor

Date

Dr. John Sullins, Committee Member

Date

Dr. Kriss A. Schueller, Committee Member

Date

Peter J. Kasvinsky, Dean of School of Graduate Studies and Research

Date

©

Susheel Vadde

2011

DEDICATION

I dedicate this thesis to my parents who have encouraged me at all phases of my life
and for their immense love on me.

ABSTRACT

Imaging biomechanical properties of biological tissues under deformation has strong implications to many medical applications such as cancer detection and surgery planning. Quantifying the elasticity of soft tissue using an optical sensor is particularly attractive because it is non-invasive and easy to operate. However, the current computing method is plagued by the existence of noises in the two-frame optical flow solutions. In this thesis, a Kalman filter based tracking algorithm is examined, aiming to improve the quality of cumulative motion over a long video sequence. The proposed method is robust and is capable of handling non-rigid motion that is typical of soft tissue. Experiments of using videos of four rat tissue specimen subject to a biomechanical tensile test indicates that the proposed tracking method is very promising in generating a smooth, accurate, and continuous multi-frame motion field. This type of multi-frame motion data not only allows us to compute a more accurate individual strain elastogram, but also provide valuable information for calibrating a series of relative strain images over the entire deformation process.

ACKNOWLEDGEMENTS

I would like to thank Dr. Zhang for giving me this opportunity to work on the biomedical imaging project and helping me to complete this thesis successfully. He has provided me tremendous encouragement and knowledge of how to approach a challenging problem by thinking beyond the box.

I would like to thank Dr. Sullins for being a great advisor during my entire graduate study at YSU and for guiding me to choose courses of my interest. I also thank Dr. Schueller for taking time from his busy schedule to serve in the thesis committee.

TABLE OF CONTENTS

ABSTRACT	V
ACKNOWLEDGEMENTS	VI
LIST OF FIGURES	VIII
LIST OF TABLES	IX
1. INTRODUCTION	1
2. RELATED WORK	2
3. EXPERIMENT DESIGN.....	4
3.1 MECHANICAL TESTING	4
3.2 VIDEO ACQUISITION AND PREPROCESSING	5
4. COMPUTING METHODS	8
4.1 TOW-FRAME MOTION BY OPTICAL FLOW ALGORITHM	8
4.2 MULTI-FRAME MOTION BY ADDITION AND KALMAN FILTER ...	10
4.3 STRAIN IMAGING BY WEIGHTED GRADIENT FILTER	13
4.4 COMPUTING TEST SETUP AND PARAMETERS	14
5. RESULTS AND DISCUSSIONS	19
5.1 MOTION TRACKING	19
5.2 STRAIN IMAGING	23
5.3 EXISTING PROBLEMS	25
6. CONCLUSIONS	26
7. REFERENCES	27

LIST OF FIGURES

FIGURE 1. EXPERIMENT SETUP	4
FIGURE 2. SAMPLES OF THE CROPPED FRAMES.	7
FIGURE 3. OPTICAL FLOW IMAGES.....	20
FIGURE 4. MULTI-FRAME MOTION FIELDS	22
FIGURE 5. THE STRAIN IMAGES.....	24
FIGURE 6. EXAMPLES OF STRAIN ELASTOGRAMS	25

LIST OF TABLES

TABLE 1. SPECIMEN VIDEOTAPING INFORMATION	6
TABLE 2. VIDEO INFORMATION WITH TOTAL/BREAK TIME AND FRAME	6
TABLE 3. KALMAN FILTER BASED TRACKING ALGORITHM	12

1. INTRODUCTION

Measuring elastic properties of biological tissues has found applications in a wide range of domains, particularly in cancer diagnosis and treatment planning. Various sensor modalities have been studied to provide quantitative measure of tissue abnormalities, including the ultrasound imaging, the magnetic resonance imaging, and the optical coherence tomography. Optical elastography is a relatively new modality that infers an object's biomechanical property variation from the observed tissue surface deformation captured in an optical video sequence. Recently, optical elastography has been used in skin diseases analysis and surgery assessment.

To generate an elastogram or strain image, an optical elastographic system must consist of three basic components: (i) A sensor that captures the tissue deformation; (ii) An algorithm that tracks the non-rigid tissue motion across multiple video frames; (iii) A forward or inverse algorithm that computes an absolute elasticity or relative strain image.

One of the main difficulties in obtaining a high-quality elastogram is that the two-frame motion (optical flow solution in this study) is often noisy, which has a severe adverse impact on elastogram quality, because the flow noise could be greatly amplified by a gradient based algorithm. The main contribution of this thesis is to utilize a Kalman filter to improve the multi-frame motion tracking and hence the elastogram quality.

The proposed method was evaluated using the videos of four rat tissue samples underwent a tensile test. Experimental results suggest that, in comparison to a simple addition method, the Kalman filter based method can produce a smooth and dense motion field over a much longer frame length that is essential for elastogram calibration.

2. RELATED WORK

There is a large body of literature on imaging tissue elasticity. In this section, a brief review of the state of the art of elastography technology is given, particularly the papers that are most relevant to this study. More comprehensive surveys and in-depth discussions can be found in [1, 2].

Since the earlier work of elastography [3, 4, 5], a large advance has been made in the algorithm development, sensor design, system integration, and clinical assessment, with a particular focus on early cancer detection and tissue characterization of internal organs, such as prostate, liver, breast, kidney, and heart [6, 7, 8, 9, 10]. The majority of the studies used either ultrasonic sensors or magnetic resonance imaging techniques. These types of modalities require direct contact of imaging sensors or excitation devices with a patient's body to generate and gather the tissue deformation data. The force applied to the tissue could be in the form of dynamic mechanical waves or quasi-static loads. However, they may not be appropriate for certain clinical situations, for example, the skin patients who suffer burn damage or are in the post-surgery recovery period.

Optical coherence tomography (OCT) has also been utilized to measure soft tissue biomechanical properties [11, 12]. An OCT based elastographic modality has the advantage that it has much higher resolution than the MRI based methods and less artifacts than the ultrasound based elastography. However, OCT based method has a drawback that its penetration depth is very limited and therefore its main application is in skin tissue characterization. Another problem of an OCT based method is that it only operates on a small surface area and also requires external excitation source to generate tissue deformation.

It is not until recently that researchers start to investigate the feasibility of *in vivo* imaging of skin elasticity using a regular optical camcorder [13, 14]. It has been demonstrated that vital information of skin tissue elasticity can be obtained with a high definition optical video acquired at a distance. Promising results have been observed in the cases of hypertrophic lichen planus, seborrheic keratosis, and psoriasis vulgaris. The optical strain images reveal the presence of significant tissue abnormalities associated with the underlying skin diseases. A similar technique based on finite element modeling and computer vision technique has also been applied to burn scar assessment [15].

One of the major obstacles in optical imaging of tissue elasticity is that the motion data computed by an optical flow algorithm is often corrupted by noise, because the algorithm is very sensitive to the illumination variation that is difficult to avoid during video recording, even in a well-control laboratory setting. One possible solution is to compute a cumulative multi-frame motion field in the framework of Kalman filter.

Kalman Filter is a mathematical tool for estimating a system's state parameters given the system's dynamic model, control inputs and noisy measurements [16]. Kalman filter has been successfully utilized in many tracking systems such as ballistic missiles and satellite navigation devices. In tissue property imaging [17], a method was developed using kalman filter and pulse echo ultrasound for detecting harmonic motion induced by ultrasonic radiation force. The method estimates the amplitude and phase of the motion at a tissue region with high sensitivity. In this study, the Kalman filter is mainly used to generate a more accurate multi-frame motion field by consolidating the noisy optical flow solutions.

3. EXPERIMENT DESIGN

3.1 MECHANICAL TESTING

Specimens of rat tissue were subject to a normal tensile test that determines the biomechanical properties. At first, a tissue sample was taken from the abdominal area of a rat and was cut into a dumbbell shape and preserved in the saline solution. An Instron Tensiometer (5500R) with a 100N load cell capable of 0.25% accuracy was used to stretch the specimen vertically. To avoid slipping effect, two grips were used to tighten the specimen to the pulling ends. The grips were also covered with aluminum foil to reduce potential contamination (see Figure 1).

The location of the bottom grip was fixed and the top grip was pulled upward at a slow and constant speed. During a tensile test, a specimen exhibited a series of sequential and gradual deformation patterns that can be characterized into three representative stages: Linear deformation, plastic deformation, and pre-rupture deformation.

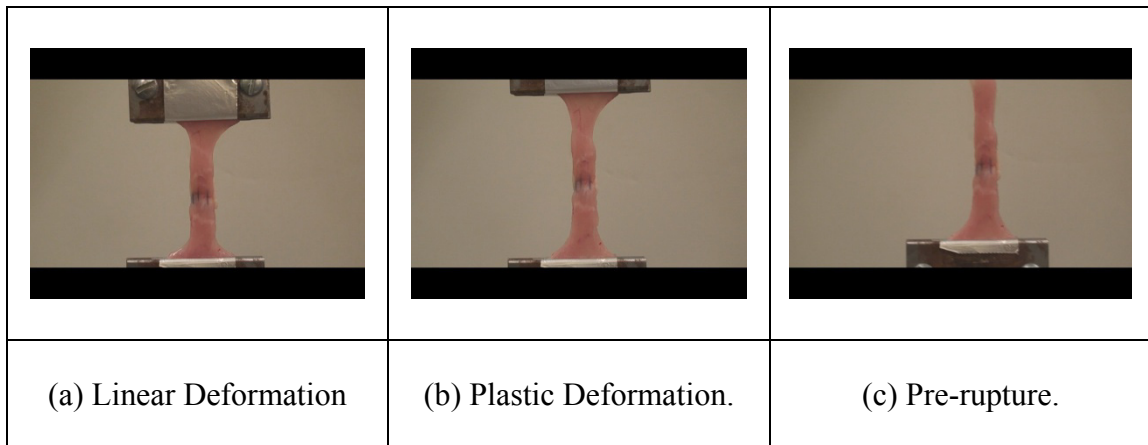


Figure 1: The illustration of the tensile experiment setup and the rat tissue deformation. The bottom grip was fixed while the top grip was pulled upward steadily until the specimen was broken. Each specimen underwent an entire deformation process that includes the linear, plastic, and pre-rupture stages.

3.2 VIDEO ACQUISITION AND PREPROCESSING

For each specimen, its entire deformation cycle was videotaped using a Sony HDR-SR1 camcorder with a capture speed of 30 frames per second. Recording condition includes a normal indoor lighting illumination and a fixed background setting in a mechanical engineering laboratory, with a constant room temperature of 25° C. The camcorder was placed at a location that was about 1.5 meter from the tensiometer. However, the focus distance of the camcorder was adjusted slightly depending upon the size of a particular specimen and the study area of interest. For example, videos of certain specimens were recorded with a zoom-in mode to capture more details of tissue deformation. Once the camcorder was focused, tension force was applied to the specimen slowly until it broke. This procedure ensured that a smooth tissue motion was obtained to facilitate the subsequent optical flow and strain computations. Of the 41 specimens that were recorded, 4 representative ones were selected in the study of motion tracking and strain imaging. Table 1 summarizes the specimen and recording information.

To perform motion tracking and strain computation, a video has to be pre-processed on the basis of individual frames. At first, all videos were split into thousands of frames using the Sony Vegas Pro-8 software package. The process can use either the start/ending times or start/ending absolute frame numbers to specify a particular video segment. The output images were in the default JPEG format. The image aspect ratio (width/height ratio) was set to 1.0 square to ensure that there was no distortion involved during the frame extraction process. Table 2 lists the time/frame statistics of the 4 videos, and Figure 2 shows a few cropped frame samples.

Table 1: Specimen Videotaping Information

Specimen ID	Recording Date	Treatment Matrix	Zoom-in View	Break Location
5A6I	9/20/2010	Yes	No	Top
5A6S	9/20/2010	Yes	No	Above Matrix
6A4S	9/21/2010	Yes	Yes	Top
6A4I	9/21/2010	Yes	No	Above Matrix

Table 2: Video Information with Total/Break Times and Frames

Specimen ID	Total # of Frames	Break Frame	Total Time	Break Time
5A6I	3479	3202	1min 56sec	1min 22sec
5A6S	3420	3058	1min 54sec	1min 48sec
6A4I	3914	3902	2min 20sec	2min 12sec
6A4S	3074	2458	1min 42sec	1min 26sec



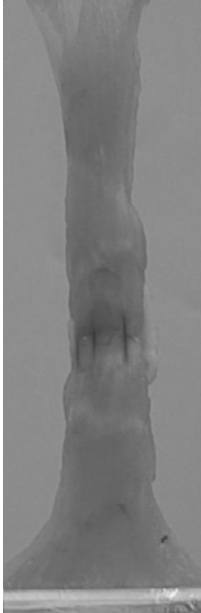
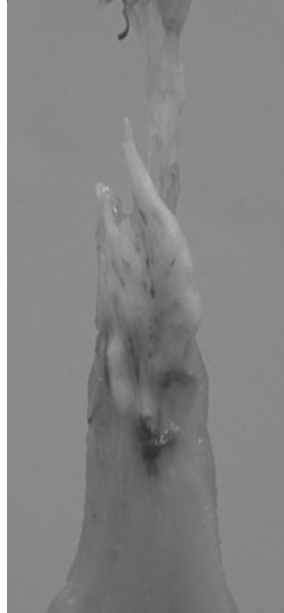



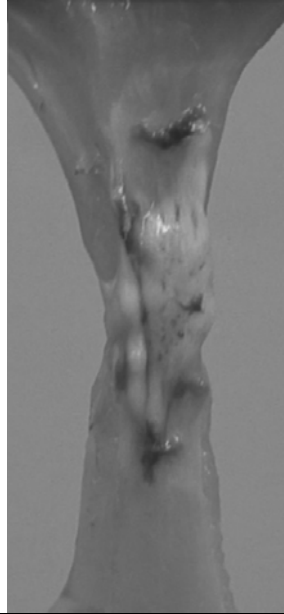
			
Frame 3450	Frame 3418	Frame 3902	Frame 3042
			
Frame 8	Frame 12	Frame 5	Frame 1
5A6I	5A6S	6A1I	6A4S

Figure 2: Samples of the cropped frames that were used in computing optical flow and strain images. Note that the background does not have a significant effect on optical flow results because of the relatively slow tissue motion.

4. COMPUTING METHODS

4.1 TWO-FRAME MOTION BY OPTICAL FLOW ALGORITHM

Optical flow represents an apparent velocity field that describes an object's motion observed in the image plane [18]. An optical flow field is obtained by solving a governing partial differential equation that is constrained by two fundamental assumptions: (i) The brightness of a material point remains unchanged between two image frames; (ii) All material points in a relatively small image neighborhood move at the same or similar speed and direction.

Considering the image brightness as a function of spatial coordinates and time, $E(x,y,t)$, then the brightness constancy between two images can be expressed as a total derivative using the well-known conservation principle:

$$\frac{dE}{dt} = 0. \quad (1)$$

For the majority of motion tracking problems, the brightness function can be treated as differentiable in both spatial and temporal domains and the equation (1) can be expanded to:

$$\frac{dE(x(t), y(t), t)}{dt} = \frac{\partial E}{\partial x} \frac{dx}{dt} + \frac{\partial E}{\partial y} \frac{dy}{dt} + \frac{dE}{dt} = 0. \quad (2)$$

In an image plane, a motion vector has two components: $U = [u, v]^T$, with $u = dx/dt$ for the horizontal motion and $v = dy/dt$ for the vertical motion. Using E_t to denote the temporal derivatives of the brightness function, the brightness constancy equation can be written in a more compact form:

$$(\nabla E)^T U + E_t = 0. \quad (3)$$

It should be noted that the PDE as expressed in equation (3) cannot be solved without ambiguity due to the lack of higher level knowledge of how an object moves in the 3D space, i.e., the aperture dilemma. To solve this problem, the brightness constancy equation must be regularized with a smoothness prior term:

$$obj(u, v) = (E_x u + E_y v + E_t)^2 + \lambda(u_x^2 + u_y^2 + v_x^2 + v_y^2), \quad (4)$$

Where E_x , E_y , u_x , u_y , v_x and v_y represent the partial derivatives of the corresponding variables, and λ is the Lagrangian multiplier (regularization coefficient). An optical flow solution (u, v) between two images can then be computed by minimizing the objective function (4). It is clear that this is a constrained solution that represents a compromise between the observed motion and the smoothness penalty.

In many situations, the two fundamental assumptions underlying the optical flow equation are often violated, especially in the presence of moving physical boundaries and depth discontinuities such as the one between a tissue specimen and the background (Figure 2). To deal with this problem, a robust algorithm is utilized that includes the piecewise smoothing and multi-resolution methods [19]. The breach of brightness constancy and spatial smoothness conditions is handled by an adaptive smoothing strategy that adjusts the penalty weight depending upon the local discontinuity property. The actual algorithm implementation can be found in [20]. In all of the experiments of this study, the optical flow parameters were pre-set based on the recommended values. But the iteration number was increased to improve the convergence performance because of the image size.

4.2 MULTI-FRAME MOTION BY ADDITION AND KALMAN FILTER

In optical flow computation, two adjacent frames were used to derive the pixel level motion field in order to satisfy the small displacement requirement of the governing equation. But the resulting two-frame flow was too small to be used in strain imaging, because the flow noise could be largely amplified by a gradient strain filter. Therefore, a tracking method is needed that calculates a larger cumulative motion by integrating multiple two-frame flows over a longer sequence.

Two tracking methods were considered: (a) A simple addition method that adds up flow results at the fixed pixel locations; (b) A robust method that is implemented in the framework a Kalman filter.

In the first method, the horizontal and vertical components of the motion vector computed from multiple frame pairs are added at each pixel:

$$u(i, i+n) = u(i, i+1) + u(i+1, i+2) + \dots + u(i+n-1, i+n) \quad (5)$$

$$v(i, i+n) = v(i, i+1) + v(i+1, i+2) + \dots + v(i+n-1, i+n) \quad (6)$$

Where $u(i, i+n)$ and $v(i, i+n)$ denote the cumulative motion between Frame i and Frame $i+n$. The cumulative motion vector will then be used to compute strain elastograms. It is difficult to estimate an optimal value of n because it depends on both an object's motion speed and the camera capture speed. In this thesis, an empirical value of 15 was used based on the results of a number of evaluation tests.

The addition method has the advantage that it is easy to implement and can process a large number of frames fairly efficiently. However, the method is based on the assumption that the motion of a physical point is relatively small, which is only valid for

a short sequence. For example, with the videos of rat tissue, 10-50 frames usually produce good tracking results. But for a longer sequence (>100 frames), the method will introduce significant artifacts and lead to poor strain images.

The Kalman filter was initially derived from linear dynamic system over discrete time domain. The state of system is defined as a vector of real numbers. A Kalman filter calculates at each discrete time interval to generate a new state from the present state. Linear operators are applied for each state with some noise measurements included.

In this study, a Kalman filter was used to integrate noisy two-frame optical flows. The method has the following advantages: (i) The measurement uncertainties (optical flow noise) is handled in a recursive prediction-correction manner that ensures an optimal tracking; (ii) The algorithm can work with a large number of points to produce a dense motion field, which is necessary for generating a strain image with a resolution close to the original input images.

The algorithm will produce an optimal estimate of a state vector by continuously updating the predictions of a process mode. It is optimal in the sense that the error covariance is minimized. A state vector (\mathbf{s}_t) is defined as: $\mathbf{s}_t = [x_t, y_t, u_t, v_t]^T$, where (x_t, y_t) and (u_t, v_t) are the true position and the true motion of a point at time t . A measurement vector (\mathbf{m}_t) is defined as: $\mathbf{m}_t = [x^*_t, y^*_t, u^*_t, v^*_t]^T$, where (x^*_t, y^*_t) is the position estimates and (u^*_t, v^*_t) is an optical flow solution. The multi-frame tracking is implemented with a recursive filter consisting of a process model and a measurement model. The process model describes the evolution of the state vector: $\mathbf{s}_t = A\mathbf{s}_{t-1} + \mathbf{q}_{t-1}$, $p(\mathbf{q}) \sim N(0, Q)$, where A is the state transition matrix, and \mathbf{q} is a zero-mean Gaussian noise with a covariance matrix Q . The measurement model relates the state vector to the noisy

flow vector: $\mathbf{m}_t = H\mathbf{s}_t + \mathbf{r}_t$, $p(\mathbf{r}) \sim N(0, R)$, where H is the identity measurement matrix, and \mathbf{r} is the measurement noise with a zero-mean Gaussian distribution and a covariance matrix R .

The tracking alternates between two stages: (i) In prediction stage, the state vector at the time t is estimated using the values obtained at the previous time $t-1$ by: $\hat{\mathbf{s}}_{t/t-1} = A\hat{\mathbf{s}}_{t-1}$. As the measurement is not used at this stage, $\hat{\mathbf{s}}_{t/t-1}$ can be viewed as the *a priori* estimate. The *a priori* error covariance matrix is computed by: $P_{t/t-1} = AP_{t-1}A^T + Q_{t-1}$, which quantifies the estimation uncertainty; (ii) In the correction stage, the Kalman gain matrix is computed by: $K_t = P_{t/t-1}H^T(HP_{t/t-1}H^T + R_t)^{-1}$, which is a blending factor that minimizes the *a posteriori* error covariance. With a blending factor, the *a posteriori* estimate of the state vector is updated by the measurement: $\hat{\mathbf{s}}_t = \hat{\mathbf{s}}_{t/t-1} + K_t(\mathbf{m}_t - H\hat{\mathbf{s}}_{t/t-1})$. The *a posteriori* error covariance matrix is also updated by: $P_t = (I - K_tH)P_{t/t-1}$. The overall Kalman filter based tracking procedure is summarizing in Table 3.

Table 3. Kalman filter based multi-frame tracking algorithm.

Stage	Equation	Interpretation
Prediction	$\hat{\mathbf{s}}_{t/t-1} = A\hat{\mathbf{s}}_{t-1}$	Predict the state (<i>a priori</i> estimate)
	$P_{t/t-1} = AP_{t-1}A^T + Q_{t-1}$	Predict the error covariance (<i>a priori</i> estimate)
Correction	$K_t = P_{t/t-1}H^T(HP_{t/t-1}H^T + R_t)^{-1}$	Compute the Kalman gain matrix
	$\hat{\mathbf{s}}_t = \hat{\mathbf{s}}_{t/t-1} + K_t(\mathbf{m}_t - H\hat{\mathbf{s}}_{t/t-1})$	Update the state vector with measurement (<i>a posteriori</i> estimate)
	$P_t = (I - K_tH)P_{t/t-1}$	Update the error covariance (<i>a posteriori</i> estimate)

4.3 STRAIN IMAGING BY WEIGHTED GRADIENT FILTER

Given a multi-frame motion field, a strain elastogram can be computed using a Cauchy strain tensor (ϵ):

$$\epsilon = \begin{bmatrix} \epsilon_{xx} = \frac{\partial u}{\partial x} & \epsilon_{yx} = \frac{1}{2} \left(\frac{\partial u}{\partial y} + \frac{\partial v}{\partial x} \right) \\ \epsilon_{xy} = \frac{1}{2} \left(\frac{\partial v}{\partial x} + \frac{\partial u}{\partial y} \right) & \epsilon_{yy} = \frac{\partial v}{\partial x} \end{bmatrix}, \quad (7)$$

where $(\epsilon_{xx}, \epsilon_{yy})$ are normal strains and $(\epsilon_{xy}, \epsilon_{yx})$ are shear strains. Since the motion vector is presented as optical flow images, spatial derivatives of the motion vector is conveniently obtained through a convolution operator:

$$\frac{\partial u}{\partial x} = S_x * u, \quad \frac{\partial v}{\partial x} = S_x * v, \quad (8)$$

$$\frac{\partial u}{\partial y} = S_y * u, \quad \frac{\partial v}{\partial y} = S_y * v, \quad (9)$$

where S_x and S_y are the weighted Sobel filters. Using the spatial derivatives of the motion vector, a strain image can be computed for each strain tensor component $(\epsilon_{xx}, \epsilon_{yy}, \epsilon_{xy}, \epsilon_{yx})$. If both horizontal and vertical strains are large, a magnitude elastogram can be obtained:

$$\epsilon_m = \sqrt{\epsilon_{xx}^2 + \epsilon_{xy}^2 + \epsilon_{yx}^2 + \epsilon_{yy}^2} \quad (10)$$

In this study, a specimen was mainly pulled vertically. As a result, the vertical strain elastogram (ϵ_{yy}) carries much more information about a sample's biomechanical property variation. For a better visualization, a strain image was also normalized to a grey scale of $[0, 255]$, with brighter/darker pixels for higher/lower strains values.

4.4 COMPUTING TEST SETUP AND PARAMETERS

A test was carried out in six steps: (1) Frame extraction; (2) Image conversion; (3) Image cropping; (4) Computing optical flows; (5) Multi-frame motion tracking; (6) Computing strain elastograms. The most computation intensive steps of optical flow and motion tracking were implemented with C/C++ and the high-level frame scheduling was managed using Perl. All tests were conducted in a Cygwin or Linux environment.

(1) Frame Extraction

1. Absolute frames of a video sequence were extracted using Sony Vegas Pro 8.
2. Parameters: HDV 1080-60i (1440 x 1080, 29.97 fps, pixel aspect ratio: 1.0).
3. The average time of extracting an entire video is about 90 minutes.

(2) Image Conversion

1. The extracted image frames are in the JPEG format.
2. JPEG images were converted to PGM format using a Perl script.

```
#!/usr/bin/perl
$src = "./6A_1I";
$dst = "./6A_1I_pgm";
opendir(DIR, "$src");
@allfiles = readdir(DIR);
$i = 0;
foreach $file (@allfiles) {
    @base = split (/_/, $file);
    if($file =~ /jpeg/) {
        system("convert $src/$file $dst/$base[0]$i.pgm");
        print "converting $file to $base[0]$i.pgm \n";
        $i = $i + 1;
    }
}
```

(3) Image Cropping

1. Purpose: remove the background that is irrelevant to tissue strain imaging.
2. Inputs: the coordinates of two controlling corner points.

```
#!/local/bin/perl
#-----
$inp = ".";
$out = "../6A_1I_pgm_cropped/1_1000/";
#-----
$start = 1;
$end = $start + 1000;
#-----Crop sub image -----
for($i = $start; $i < $end; $i++){
    $name = "Image$i";
    system("../Rat_Code_Crop/crop $name.pgm 708 386 788 918 ");
    print "cropping $name \n";
}
system("mv cropped*.pgm $out");
print "Finish moving images. \n";
```

(4) Computing Optical Flow

1. This is the most time consuming step.
2. Inputs: cropped images indexed by two integer numbers.
3. Key parameters: Iteration number = 20, Stages = 5, Frame interval = 1.
4. Outputs: Image/text files of motion vector in horizontal/vertical directions.

Specimen	No of Frames	No. of Frames Tracked	Computing Time
5A6I	3479	800	14 hrs 20 min
5A6S	3420	800	14 hrs 7 min
6A4I	3712	800	14 hrs 37 min
6A4S	3074	800	14 hrs 25min


```

#!/local/bin/perl

$rows = 791;
$cols = 171;

$interval = 1;
$skip = 0;

$start = 1;
$end = $start + 20;
#-----
$src = "./6A_1I_pgm_cropped/1_20";
$dst = "./6A_1I_pgm_cropped_flow/1_20";
#-----
for($i = $start; $i < $end; $i++){
    $j = $i + $interval;
    system("../Rat_Code_Flow/src/gnc $i $j 4 1 $src/cropped_Image $dst/flow-
$i-$j- -l1 10.0 -l2 1.0 -S1 10.0 -S2 1.0 -s1 10.0 -s2 0.05 -stages 5 -nx $cols -ny
$rows -f 0.5 -F 0 -w 1.995 -iters 20 -end '.pgm' -skip 15");
    print "optical flow: $i $j \n";
    $i = $i + $skip;
}
#----- Delete unused files -----
system("rm $dst/*-0.*");
system("rm $dst/*-1.*");
system("rm $dst/*-2.*");
system("rm $dst/*-3.*");
system("rm $dst/*-data-*");
system("rm $dst/*-spatial-*");
system("rm $dst/*-stable-*");
system("rm $dst/*.hdr*");

#----- Move Text files -----
system("mkdir $dst/text");
system("mkdir $dst/u_flow");
system("mkdir $dst/v_flow");

system("mv $dst/*.txt $dst/text/");
system("mv $dst/*-u-*.pgm $dst/u_flow/");
system("mv $dst/*-v-*.pgm $dst/v_flow/");

```

(5) Motion Tracking

1. Both Addition method and Kalman filter method were used.
2. Inputs: multiple optical flow fields to be tracked.
3. Parameters: boundary width (BD), smoothing window, starting/ending frames.

```
#!/local/bin/perl

$rows = 791;
$cols = 111;
$skip = 0;
$BD      = 40;
$nSmooth = 1;
$smooth_halfWin = 2;

#-----
$src = "/6A_1I_pgm_cropped_flow/1_2000/text";
$dst = "/6A_1I_pgm_cropped_flow_track/1_2000";
system("mkdir $dst");
#-----

$startID = 500;
$endID   = $start + 995;

#-----          exe src dst startID endID rows cols BD
nSmooth smooth_halfWin stage
system("../Rat_Code_TRACK_Flow/TRACKFLOW $src $dst $startID
$endID $rows $cols $BD $nSmooth $smooth_halfWin 4  ");

#----- Move files -----
system("mkdir $dst/track_text");
system("mkdir $dst/track_u");
system("mkdir $dst/track_v");

system("mv $dst/*.txt  $dst/track_text/");
system("mv $dst/*-u*.pgm $dst/track_u/");
system("mv $dst/*-v*.pgm $dst/track_v/");
#-----
```

(6) Computing Strain Images

1. The strain image was computed using a gradient filter.
2. Inputs: multi-frame motion field.
3. Parameters: FDorSobel: 1 for finite difference method and 2 for Sobel filter.
4. Outputs: a strain elastogram.

```
#!/local/bin/perl
$rows = 791;
$cols = 171;
$exe = "../Rat_Code_Strain/STRAIN";
$inpdire = "/5A_6S_pgm_cropped_flow/3000_4000/addflow/addflow_text";
$outdire = "/5A_6S_pgm_cropped_strain";
system("mkdir $outdire");
$nSmooMot = 0;
$nSmooStr = 0;
$conWidth = 1;
$halfWin = 1;
$fbd = 50;
$sbdtop = 210; $sbdbot = 20;
$sbdleft = 20; $sbdright = 15;
$fdorsobel = 1;
#-----
opendir(DIR, "$inpdire");
@allfiles = readdir(DIR);

foreach $file (@allfiles) {
    if($file =~ /-U/) {
        @token = split(/\./, $file);
        $base1 = $token[0]; $base2 = $token[1]; $base2 =~ s/-U/-V/;
        # exe base1 base2 inpdire outdire rows cols nSmooMot nSmooStr
        conWidth halfWin fbd sbdtop sbdbot sbdleft sbdright
        fdorsobel
        system("$exe $base1 $base2 $inpdire $outdire $rows $cols $nSmooMot
        $nSmooStr $conWidth $halfWin $fbd $sbdtop $sbdbot $sbdleft
        $sbdright $fdorsobel");
        print "$exe $base1 $base2 $inpdire $outdire $rows $cols $nSmooMot
        $nSmooStr $conWidth $halfWin $fbd $sbdtop $sbdbot $sbdleft
        $sbdright $fdorsobel \n\n";
    }
}
```

5. RESULTS AND DISCUSSIONS

5.1 MOTION TRACKING

The two-frame motion fields computed with the optical flow algorithm are quite noisy (see Figure 3). In the vertical flow images, darker pixels indicate the upward motion and brighter pixels indicate downward motion. In the horizontal flow images, darker pixels suggest the motion to the left and brighter pixels are for the motion to the right. It should be noted that the motion values at all pixels in an image are normalized to a grayscale of 0 to 255. Therefore, a flow image is of relative meanings only. In other words, a vertical flow image and a horizontal flow images cannot be compared on the basis of their absolute pixel intensity values. In fact, since the tissue deformation in a tensile test is dominated in the vertical direction, the magnitude of vertical motion is much larger than that of its horizontal counterpart.

Several observations can be made from the two-frame optical flow results: (i) The motion vector has been successfully computed (both horizontal and vertical components), although data quality is compromised by flow noise; (ii) Since the difference between the horizontal and vertical components could be of several orders of magnitude, the strain images will be primarily influenced by the vertical component; (iii) Computing an optical flow using the two adjacent frames satisfies the small displacement condition of the governing equation. However, the motion values are in the sub-pixel level (< 0.4 pixel), which makes it vulnerable to random noise. One possible solution is to use larger frame interval without violating the constraint condition, which will be investigated in future studies; (iv) Including the background in the cropped images does not seem to have a significant impact on the flow results, probably due to the small two-frame deformation.

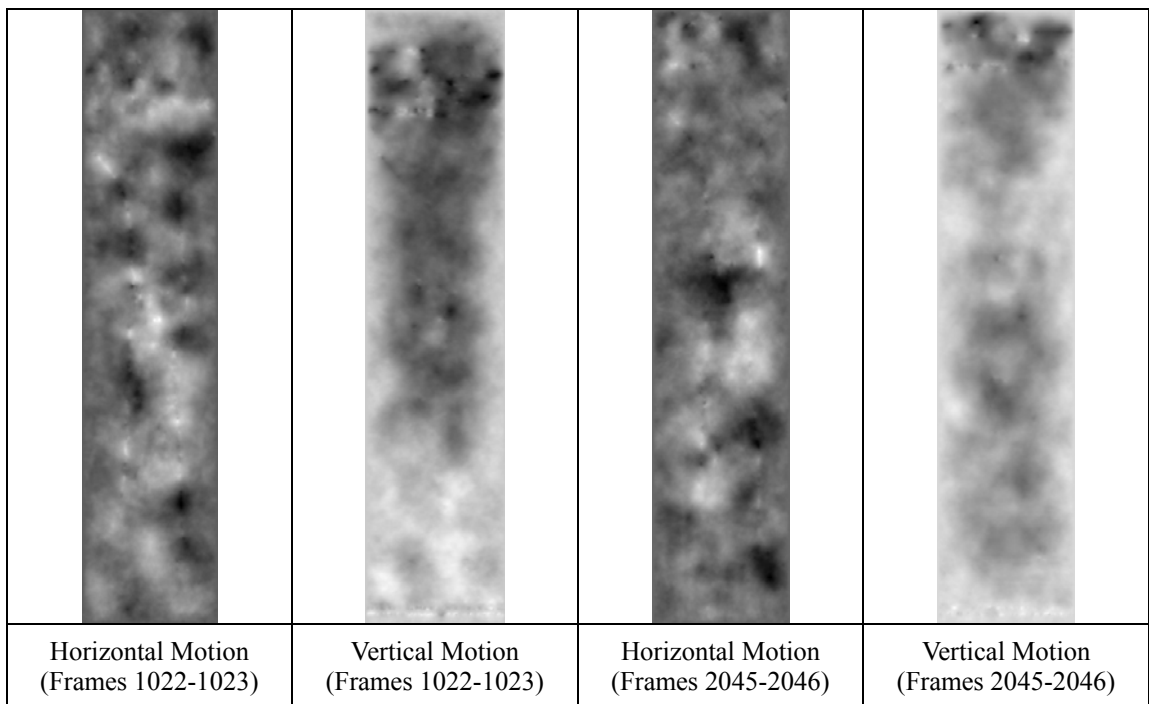
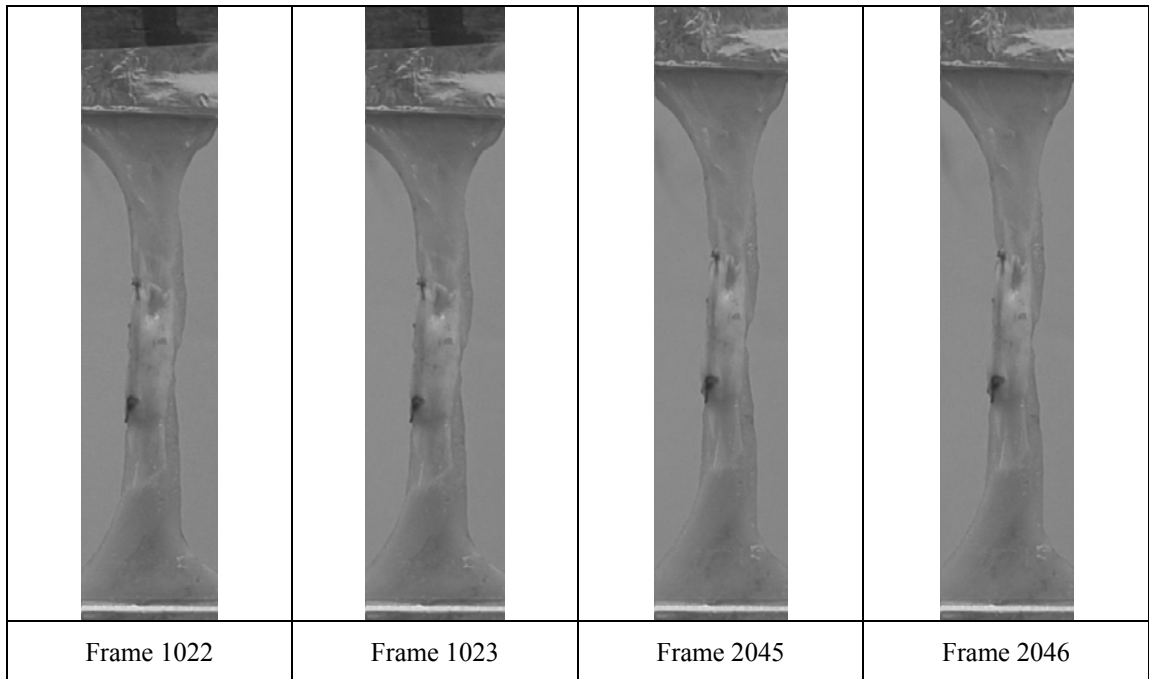


Figure 3: Sample frames from the videos of specimen 6A11 and the corresponding two-frame optical flow results. The geometry of the specimen can be roughly identified in the flow images that are generally noisy.

Figure 4 shows the multi-frame tracking results using the addition method and the Kalman filter based method. The darker pixels indicate upward or leftward motion and brighter pixels indicate downward or rightward motion, respectively, with the intensity values proportional to the motion magnitude.

For the addition method (Figure 4, top row), 15 frames were added to generate a multi-frame motion. It is apparent that the motion quality is much improved as evidenced by the smoother image intensity, in comparison to the two-frame flow images. If a flow image can be modeled as motion signal plus the white noise, adding multiple flow images at the fixed pixels clearly averaged out the random noises. Because the two-frame flow results show much larger noises at the boundary, 30-50 boundary pixels were cut off to minimize the noise effect (the black pixels).

Large improvements were also observed in the multi-frame motion images computed using the Kalman filter algorithm (Figure 4, bottom row). Given a short video segment (frames 1-16 for the addition method and frames 1-33 for Kalman filter method), both approaches produced good results. However, only the Kalman filter method is capable of handling a long sequence that captured the entire tissue deformation (linear stage, plastic stage, and the pre-rupture stage). For example, the cumulative motion of more than 3,000 frames (6A1I) has been tracked with a good quality. This type of tracking over a large number frames is very useful in matching the stress-strain history, which can be further utilized in strain calibration. Some of the feature points were lost during the Kalman filter tracking. This problem can partially be solved by recovering the lost points (e.g., assigning the average motion values of its neighboring points).

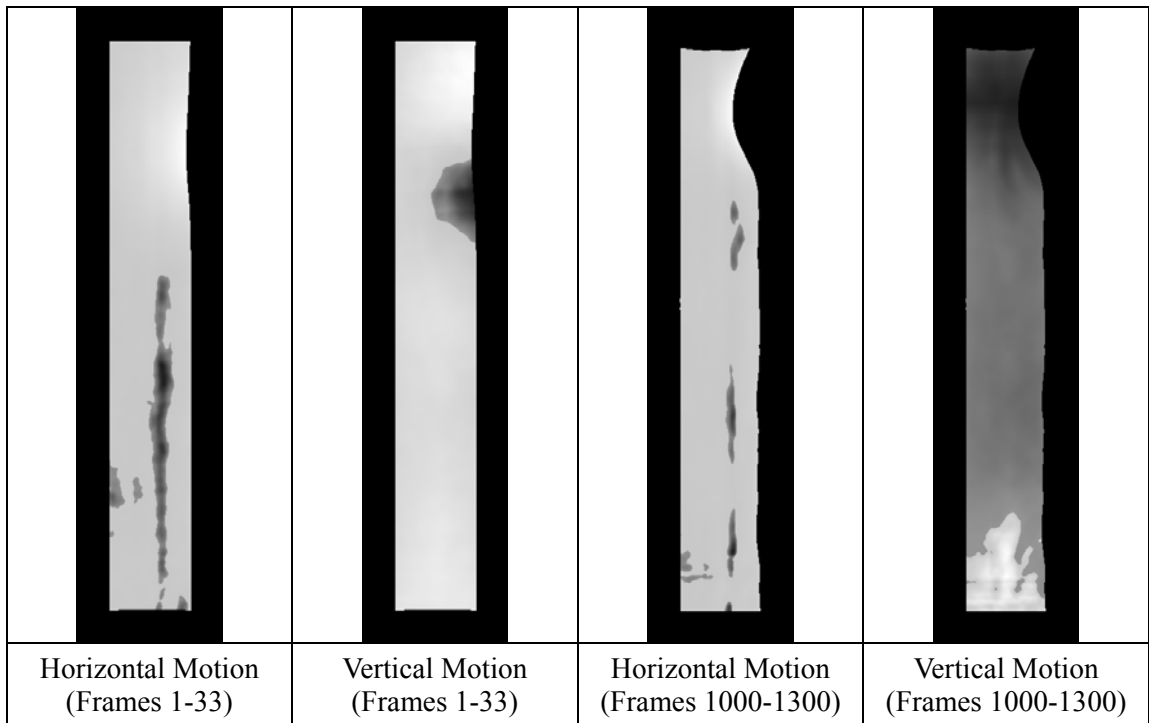
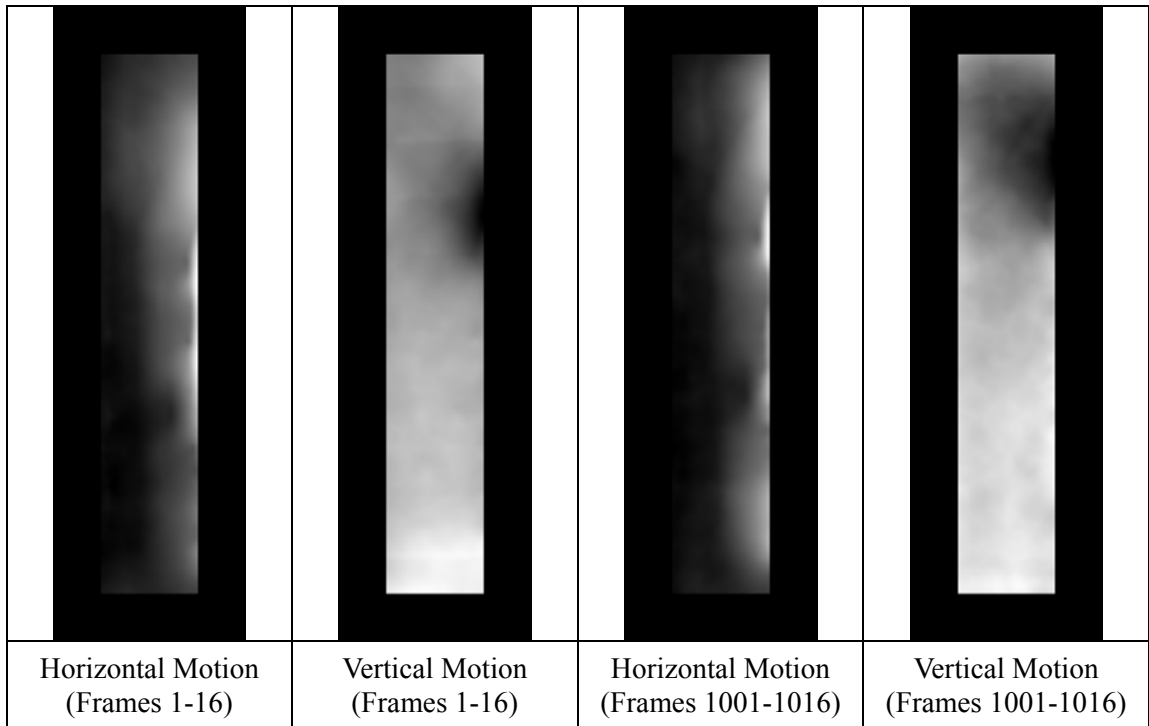


Figure 4: Multi-frame motion fields computed using a simple addition method (top row) and a Kalman filter based robust tracking algorithm (bottom row).

5.2 STRAIN IMAGING

Given the multi-frame motion fields tracked by either the addition method or the Kalman filter method, strain elastograms can be obtained by applying the weighted gradient filter to the motion data (see Figure 5).

For a short sequence (15 frames and 33 frames), both tracking methods resulted in good strain images of similar patterns that characterize the tissue matrix. For example, the muscle structure (layers of fibers) is clearly visible, which is indicative of the existence of material property heterogeneity that is difficult to see in the raw images. Due to the lack of quantitative measurement of collagen and elastin fibers of the specimen, it is not clear yet whether the observed strain patterns can be correlated to the property variations in different deformation stages (linear, plastic, and pre-rupture). In future investigations, it is highly desirable to establish a quantitative correlation based on the tests of a large number samples, so that a strain elastogram can be interrelated with a sound biophysical support, at least on the level of collagen and elastin fibers that play the major role in determining tissue elasticity.

The strain images of a long sequence (300 frames) tracked by the Kalman filter is somewhat different from that of a short segment (15 frames) by the addition method, with the former showing more disparity in strain values at the top and middle sections, which is more descriptive of the tissue deformation history over time. It should be emphasized that both types of strain elastograms provide valuable information of tissue property changes associated with the pathological process and hence have great potentials in revealing diseased induced tissue abnormalities.

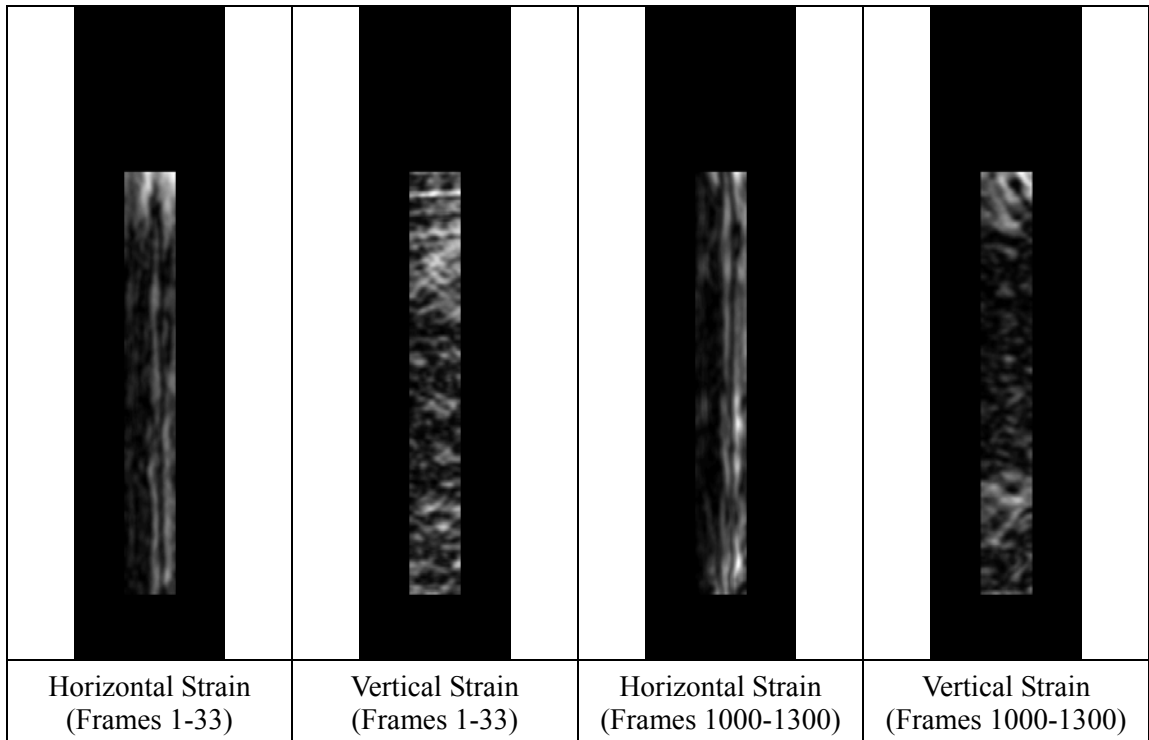
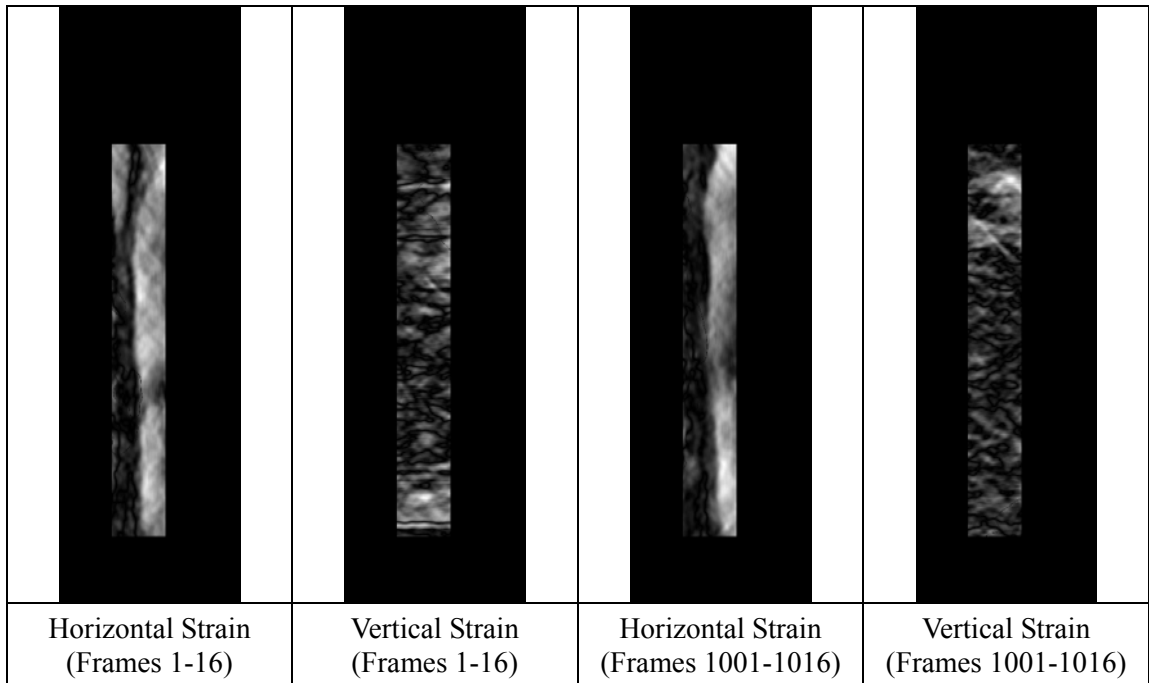


Figure 5: The strain images derived from the multi-frame motion tracked by the addition method (top row) and a Kalman filter algorithm (bottom row). All images were computed using the videos of 6AIS.

5.3 EXISTING PROBLEMS

Since optical elastography is still in its early developing stage, there are many technical issues that need to be addressed before it can be used in a clinical trial and eventually real medical applications. A large number of evaluation tests have to be conducted using various tissue samples. In this study, it was found that, for certain video frames, the strain elastograms using the tracking data of the addition method had artifacts in the forms of salient irregular curves (Figure 6, image on the right). It is not clear what causes the artifacts that might be related to the smoothing operators or boundary effect. Another problem is that the feature points could be lost during Kalman filter tracking as seen in Figure 4. All of those issues need to be addressed in future investigations.

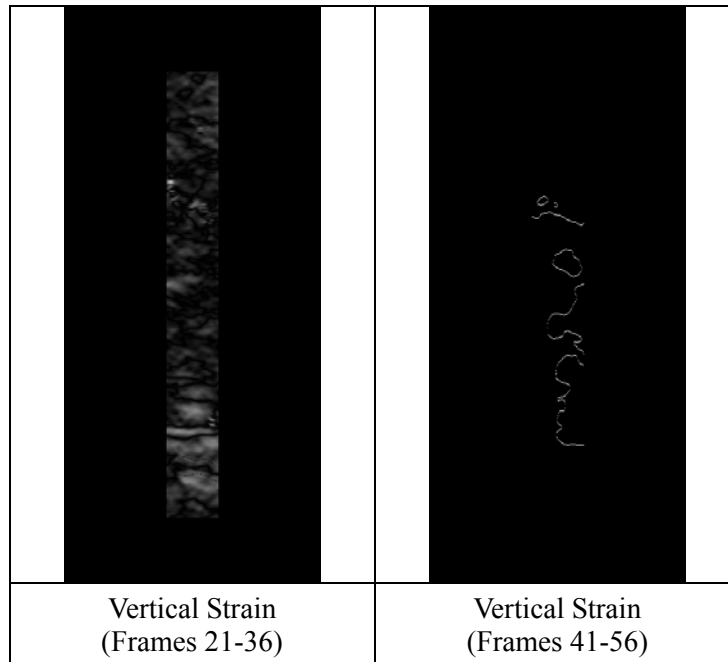


Figure 6: Examples of strain elastograms with and without artifacts using the addition method (the vertical strain component of frames 41-56 from specimen 6A4S).

6. CONCLUSIONS

This thesis investigates the feasibility of using a Kalman filter based approach to improve the quality of motion tracking over a long video sequence and the subsequent strain elastogram computation. The experiments were carried out using the optical videos of rat tissue that were subject to a normal biomechanical tensile test. Given the noisy two-frame optical flow solutions, the proposed Kalman filter based tracking algorithm proves to be a very promising approach in minimizing the impact of flow noise and providing a stable and accurate estimation of tissue deformation. In comparison to the addition method, the Kalman filter method has the advantage that it is capable of tracking a very long video sequence without causing a severe deviation. More importantly, the strain elastograms derived from the long tracked multi-frame motion field has significant implications to both basic medical imaging research and clinical applications.

7. REFERENCES

- [1] Ophir J, Alam SK, Garra BS, Kallel F, Konofagou EE, Krouskop T, Merritt CRB, Righetti R, Souchon R, Srinivasan S, and Varghese T, Elastography: Imaging the elastic properties of soft tissues with ultrasound, *Journal of Medical Ultrasonics*, 2002; 29 (Winter): 155-171.
- [2] Parker KJ, Doyley MM, and Rubens DJ, Imaging the elastic properties of tissue: the 20 year perspective, *Physics in Medicine and Biology*, 2011; 56: R1-R29.
- [3] Ophir J, Cespedes I, Ponnekanti H, Yazdi Y, and Li X, Elastography: A quantitative method for measuring the elasticity of biological tissues, *Ultrasonic Imaging*, 1991; 13: 111-134.
- [4] Parker KJ, Huang SR, Musulin RA, and Lerner RM, Tissue response to mechanical vibrations for “sonoelasticity imaging”, *Ultrasound in Medicine and Biology*, 1990; 16: 241-246.
- [5] Muthupillai R, Lomas DJ, Rossman PJ, Greenleaf JF, Manduca A, and Ehman RL, Magnetic resonance elastography by direct visualization of propagating acoustic strain waves, *Science*, 1995; 269: 1854-1857.
- [6] Krouskop TA, Wheeler TM, Kallel F, Garra BS, and Hall TJ, The elastic moduli of breast and prostate tissues under compression, *Ultrasonic Imaging*, 1998; 20: 260-274.
- [7] Righetti R, Kallel F, Stafford RJ, Price RE, Krouskop TA, Hazle JD, and Ophir J, Elastographic characterization of HIFU-induced lesions in canine livers, *Ultrasound in Medicine & Biology*, 1999; 25: 1099-1113.

- [8] Garra BS, Céspedes I, Ophir J, Spratt S, Zuurbier RA, Magnant CM, and Pennanen MF, Elastography of Breast lesions: initial clinical results, *Radiology*, 1997; 202: 79-86.
- [9] Weitzel WF, Kim K, Rubin JM, Xie H, and O'Donnell M: Renal advances in ultrasound elasticity imaging: measuring the compliance of arteries and kidneys in end-stage renal disease, *Blood Purification*, 2005; 23:10-17.
- [10] Konofagou EE, D'hooge J, and Ophir J, Myocardial elastography, A feasibility study in vivo, *Ultrasound in Medicine and Biology*, 2002; 28: 475-482.
- [11] Ko HJ, Tan W, Stack R. Boppart SA, "Optical Coherence Elastography of Engineered and Developing Tissue", *Tissue Engineering*, 2006; 12: 63-73.
- [12] Sun C, Standish B and Yang VXD, Optical coherence elastography: current status and future applications, *J. Biomed. Opt.* 16, 043001 2011.
- [13] Zhang Y., Brodell R. T., Mostow E. N., Vinyard C. J., and Marie H., In vivo skin elastography with high definition optical videos, *Skin Research and Technology*, 2009; 15: 271-282.
- [14] Zhang Y, Sullins JR, Goldgof DB, Manohar V, Computing strain elastogram's of skin using an optical flow based method, *Proceed. of 5th Inter. Conf. on Ultrasonic Measurement and Imaging of Tissue Elasticity*, Snowbird, Utah, October, 2006.
- [15] Zhang Y, Goldgof DB, Sarkar S, Tsap LV. A modeling approach for burn scar assessment using natural features and elastic property, *IEEE Transactions on Medical Imaging*, 2004; 10:1325-1329.

- [16] Kalman RE, A New Approach to Linear Filtering and Prediction Problems, Transactions of the ASME - Journal of Basic Engineering, 1960; 82: 35-45.
- [17] Yi Zheng, Shigao Chen, Wei Tan, Kinnick R. Greenleaf JF, Detection of tissue harmonic motion induced by ultrasonic radiation force using pulse-echo ultrasound and kalman filter, IEEE Transactions on Ultrasonics, Ferroelectrics and Frequency Control, 2007: 54: 290-300.
- [18] B. K. P. Horn and B. G. Schunck, Determining optical flow, AI Memo 572, Massachusetts Institute of Tech., 1980.
- [19] M. J. Black, P. and Anandan, The robust estimation of multiple motions: parametric and piecewise-smooth flow fields, Computer Vision and Image Understanding, 1996; 63: 75-104.
- [20] <http://www.cs.brown.edu/~black/>